



HAL
open science

Influence of the tufting pattern on the formability of tufted multi-layered preforms

Hao Shen, Peng Wang, Xavier Legrand, Lingshan Liu, Damien Soulat

► To cite this version:

Hao Shen, Peng Wang, Xavier Legrand, Lingshan Liu, Damien Soulat. Influence of the tufting pattern on the formability of tufted multi-layered preforms. *Composite Structures*, 2019, *Composite Structures*, 228, 10.1016/j.compstruct.2019.111356 . hal-04548229

HAL Id: hal-04548229

<https://hal.univ-lille.fr/hal-04548229v1>

Submitted on 29 Nov 2024

HAL is a multi-disciplinary open access archive for the deposit and dissemination of scientific research documents, whether they are published or not. The documents may come from teaching and research institutions in France or abroad, or from public or private research centers.

L'archive ouverte pluridisciplinaire **HAL**, est destinée au dépôt et à la diffusion de documents scientifiques de niveau recherche, publiés ou non, émanant des établissements d'enseignement et de recherche français ou étrangers, des laboratoires publics ou privés.



Distributed under a Creative Commons Attribution - NonCommercial 4.0 International License

Influence of the tufting pattern on the formability of tufted multi-layered preforms

Shen Hao¹, Peng Wang^{1,*}, Xavier Legrand¹, Lingshan Liu², Damien Soulat¹

¹ *University of Lille, Ensait, Gemtex, F-59000 Roubaix, France*

² *School of Textile Science and Engineering, Wuhan Textile University, China*

* Corresponding author. Tel.: +33 3 20 25 89 47. Fax.: +33 3 20 25 64 61.

E-mail address: peng.wang@ensait.fr

Abstract: As a relatively novel technique, tufting is recently used to provide through-thickness reinforcement of a traditional 2D multi-layered preform, thus improving its resistance to delamination in the final part. In order to optimize the manufacturing process of the composite preforms reinforced by tufting, the studies of the forming behaviour of these tufted preforms are quite necessary, in particular, the influence of the tufting pattern. The present paper investigates the formability of the circle-spiral and square-spiral tufted preforms during the hemispherical and square-box forming. The forming defects and the consistency between the tufting pattern and punch shape are mainly discussed. The experimental assessment demonstrates that the tufting pattern has an impact on the formability of tufted preform and can modify/remove the forming defects. Moreover, there is no significant importance to use the similar tufting pattern to the punch shape and the forming results depend on the number of the tufting points in the zone underlying the blank holder.

Keywords: Fabrics/textiles; Multi-layered preform; Forming; Tufting

1. Introduction

Recently, textile-reinforced composites have been gain more and more attention in the aerospace, automobile and transportation industries since they can not only provide almost identical mechanical performances compared to metallic materials in some structural applications but also further reduce total weight. Especially for the woven composites, owing to its high flexibility of the fibre reinforcement, they can be directly manufactured to the final shape without extra assembly operations[1]. Thus, they are able to be widely used as alternatives to replace metal parts for advanced structures.

Resin Transfer Molding (RTM) is one of the main manufacturing processes for the production of composite parts [2,3]. As the first step of the RTM process, the dry fabrics should be shaped by a forming machine including punch, die and blank-holder components. This forming process can induce a complex variation of physical behaviours and mechanisms influencing the next manufacturing stage (resin infusion/injection stage). Many input parameters have a strong impact on this step, such as the architecture of reinforcement, punch shape, blank-holder pressure, the orientation of yarns, etc.[4–12]. Therefore, many experiments need to be carried out in order to take into account the influence of the process parameters. Some previous experimental works [4–12] have illustrated the measurement criteria which can be used in the quantification of the formability behaviours of dry textile reinforcements such as material draw-in, interlayer sliding and homogeneity of fibre density. Forming defects (wrinkling[6,13–16], buckling[17], misalignment of fibres[11], etc.), which are not acceptable for the final composite part, may be related to these formability behaviours to some extent. Furthermore, the number of experimental tests can be reduced by using finite element simulation tools [11,18–21].

In the multi-layered dry fabric forming, the number of layers, layer orientations and stacking sequence are important parameters, as they are strongly related to the loads on the

contact surfaces between the layers during forming. Due to the existence of these interlayer effects, forming of quasi-isotropic lay-up is hard to avoid the occurrence of wrinkling phenomenon in the final part[7,22]. Some numerical and experimental works have proved that friction plays a significant role during multilayer forming [23–26]. Meanwhile, the multilayer preforms are also quite sensitive to the interlayered slippage. Therefore, through-the-thickness reinforced preforms which can be realized by different technologies (such as 3D weaving, stitching, tufting, and Z-pinning[27–33]) are proposed to solve this problem. Some experimental studies have been carried out to investigate the deformability and mechanical properties of 3D woven interlock preform [5,32]. Some works about the effect of stitching patterns on the sample forming behaviours have proved that high stitch density can reduce the material draw-in measurement value and fabric shearing. However, these studies are limited to the stitching process and few works are dedicated to the tufted preforms, especially to the investigation of the effect of tufting parameters on forming defects. Liu et al[34] found that tufting technique can improve the formability behaviours of tufted multi-layered preforms. Nevertheless, the influence of tufting patterns, as tufting density and tufting shape, on the deformability was not fully studied.

The aim of this study is to further improve the understanding of the effects of different tufting parameters on formability behaviours of multi-layered preforms. Two primary tufting patterns (the circle spiral and the square spiral), corresponding to the punch shapes (hemispherical and square-box), were tested to investigate the necessity of the consistency of tufting pattern and punch shape. Moreover, the formability behaviours were systematically analysed through these two patterns with different tufting density in both hemispherical and square-box forming.

2. Methods and materials

2.1 Tufting process

Tufting technology based on conventional stitching process was invented originally for the manufacture of carpet and recognized recently as an important way to develop the through-the-thickness reinforcement of composites [35,36]. The schema of tufting is demonstrated in Fig.1. Thanks to a hollow needle, the thread is inserted into the dry preform through the thickness from only one side without any tension. This tension-free thread introduction system can reduce the degradation of the in-plane properties during the forming of loops. The tuft loop can be maintained in the preform (Partially inserted tuft) or the needle inserts through the whole thickness (Fully inserted tuft) [27]. Compared to the stitching technology, tufting is simpler as it does not need two threads to interlock at two sides of the preform [34].

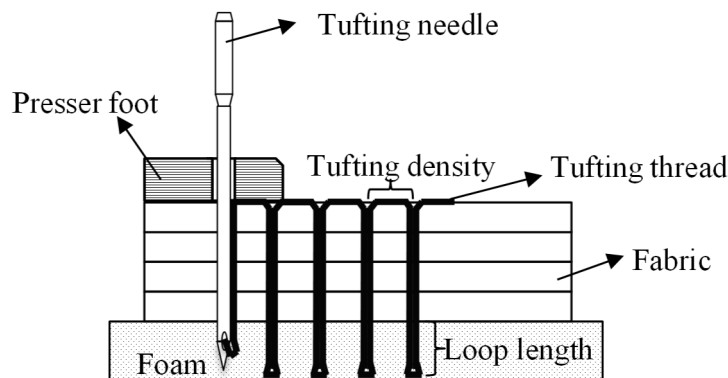


Fig.1. Schema of the tufting process.

Several industrial devices were designed to automate the tufting process and to achieve the trajectory tracking with the help of a robotic manipulator [35–38]. Equipment shown in Fig.2a was developed by GEMTEX laboratory to carry out the tufting process. As the main part of the equipment, tufting head is assembled with a tufting needle linked with a pneumatic jack to control the needle stroke. Thread feeding device ensures a smooth supply of the tufting thread with a certain length and tension. [Presser foot device applies a constant pressure on the fabric before the tufting needle starts penetrating, and it is released until the tufting needle retracts](#)

fully from the fabric. The framework provides all movements of tufting head along the X and Y axes. The tufting routines and the tufting parameters, such as tufting deepness, tufting pattern and tufting density can be controlled.

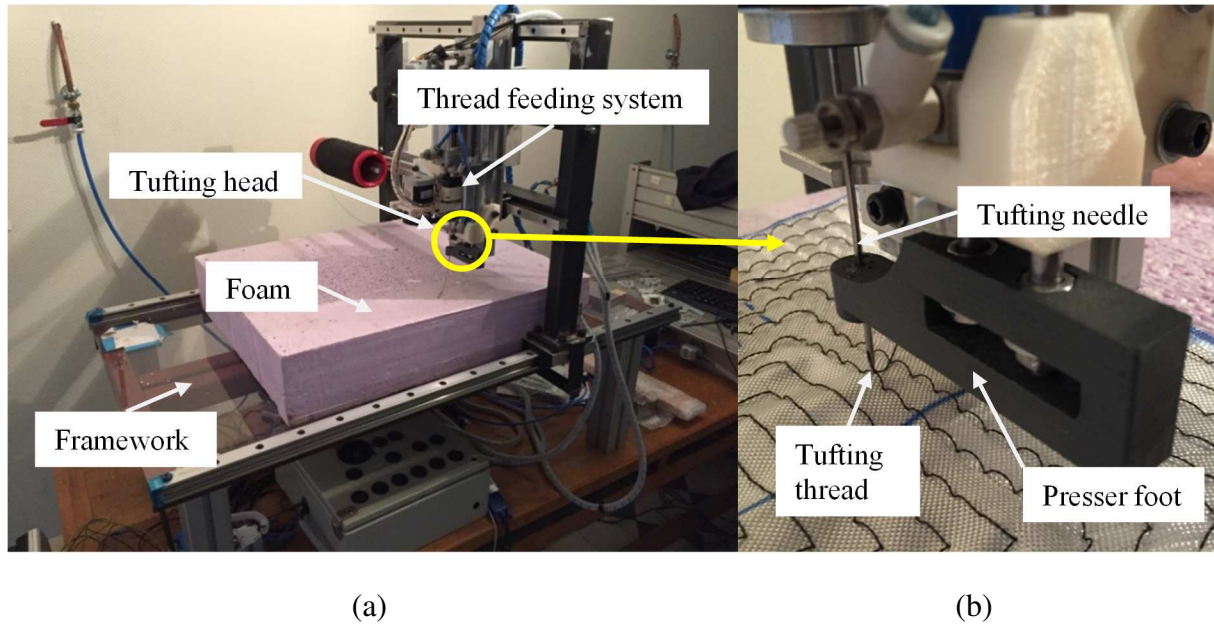


Fig. 2 Tufting device (a) and zoom of tufting head (b).

2.2 Forming device

Fig. 3 shows the forming device used in the present study to characterize the textile reinforcements formability [5,34,39]. The punch/open-die system can be easily changed to obtain different double curvature shapes. The punch is controlled by an electric jack to reach its target location at a given speed. A load sensor ($500\text{N} \pm 0.3\%$) records the variation of the punch load during the preforming. A continuous video to record the forming process is shot by a digital camera installed above the specimen. The maximum material draw-in and the maximum inter-layer sliding used in this study can be measured by the image extracted from this video using ImageJ. The pre-tensioning system consists of four pneumatic jacks and two transparent blank-holders. This system permits to apply an adjustable pressure on the fabric. The geometry of the blank-holders can be changed easily according to the punch shape.

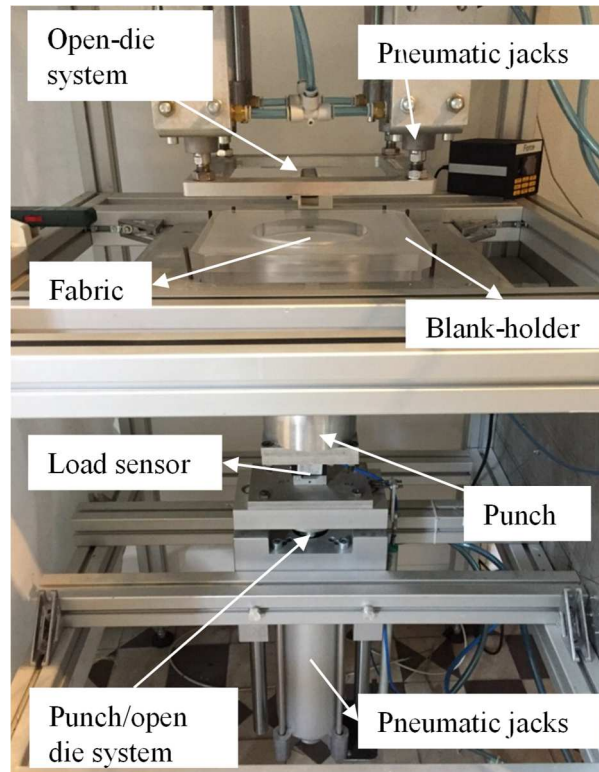


Fig. 3. The forming device.

A hemispherical punch and a square-box punch were chosen in the present study to investigate the influence of different tufting patterns on the formability of tufted preforms. The punch displacement is a constant value which depends on the punch shape. The main dimensions and forming parameters are noted in Fig. 4 and Table.1. The punch pressure and the blank-holder pressure represent the values of the air pressure supplied to the punch and blank-holder respectively. The stamping speed is measured when no sample is used.

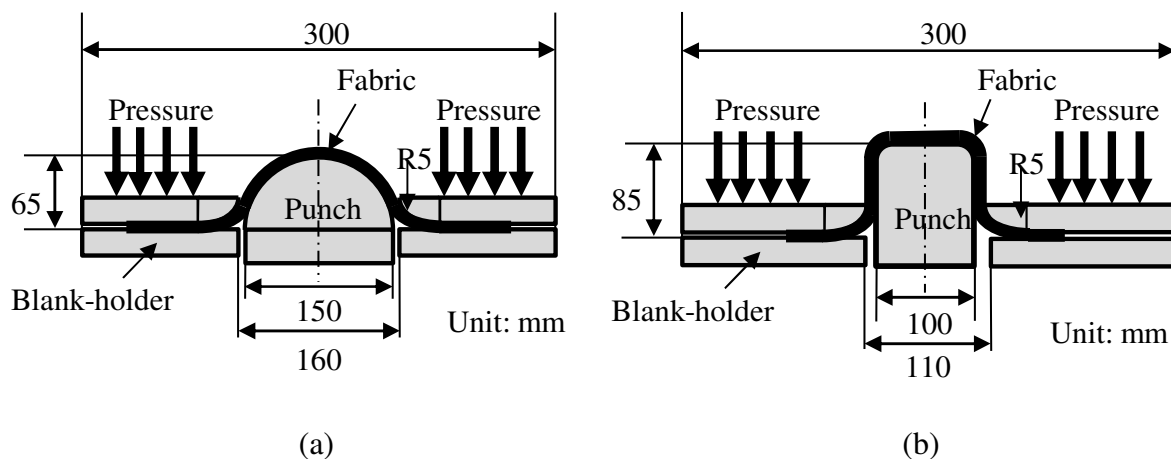


Fig.4. Schematic of forming device: (a) Hemispherical punch (b) Square-box punch

Table 1 Main parameters of the forming process.

Parameter	Value
Stamping speed	45 mm/s
Blank-holder pressure	0.05 MPa
Punch pressure	0.2 MPa

2.3 Materials

E-glass plain woven fabric with an areal density $157 \pm 5 \text{ g/m}^2$ was used in the forming tests. The preform with a sequence of $[0^\circ/90^\circ, \pm 45^\circ]_2$ is chosen in the present study. The dimensions of the tested preforms are $280 \times 280 \text{ mm}^2$, with a thickness of $1.1 \pm 0.1 \text{ mm}$. All the samples were tufted with TENAX[®] carbon thread (67 tex) into two different patterns, via a hollow needle of 2 mm diameter. The tufting patterns are figured out in Figs. 5a and 5b: square spiral and circle spiral. As the important tufting parameters, the tufting space and tufting angle are defined in Fig. 5. Tufting starts from the centre of the preform to assure that only one tufting thread is used to insert continuously in both warp and weft directions.

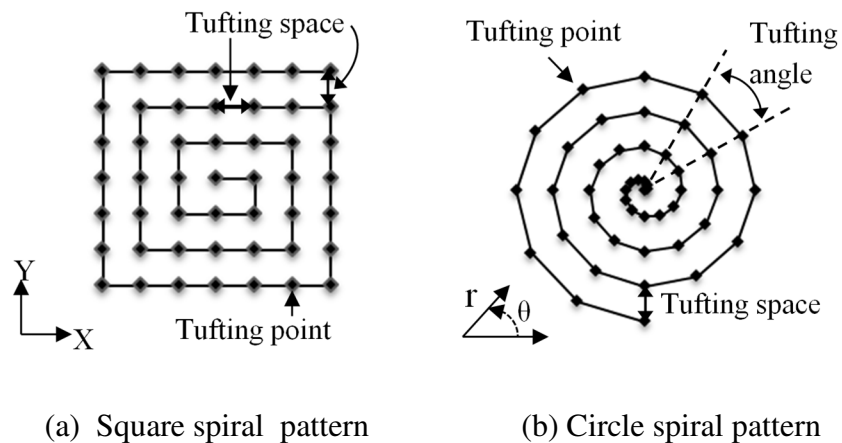


Fig. 5. Schematic description of the different tufting patterns.

Cartesian coordinate system (Fig. 5a) is chosen for tufting in the square spiral to specify the tufting point, which keeps a constant tufting space in X and Y axes. The circle spiral (Fig. 5b) is known as the Archimedean spiral, described by the equation (1) in polar coordinates (r, θ) .

$$r(\theta) = \frac{d}{2\pi} \times (n-1) \times \theta \quad (1)$$

where d is the tufting space between successive turnings; n is the serial number of tufting point on the spiral lattice; θ is the tufting angle between successive tufting points. Top view of tufted samples using the square spiral and circle spiral tufting patterns are shown in Fig. 6.

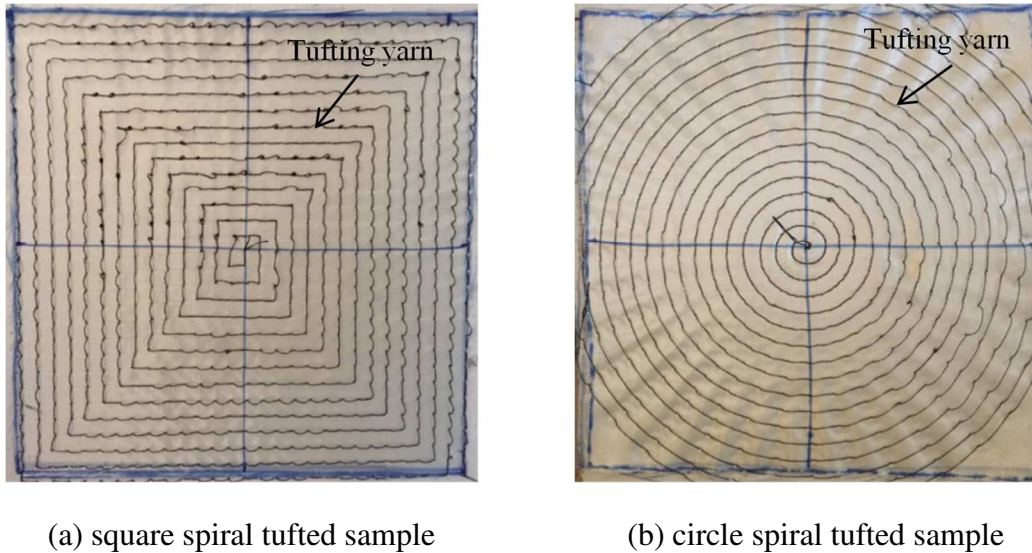
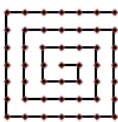



Fig. 6. Top view of the tufted preforms with the different tufting pattern.

Table. 2 lists the main properties of tufted 3D preforms used in the present study. The samples of square spiral pattern with the variation of tufting space and of circle spiral pattern with the variation of tufting space and tufting angle were prepared for the forming tests. As the length of the inserted thread is a constant, the areal density depends on the tufting space/angle and the number of tufting points.

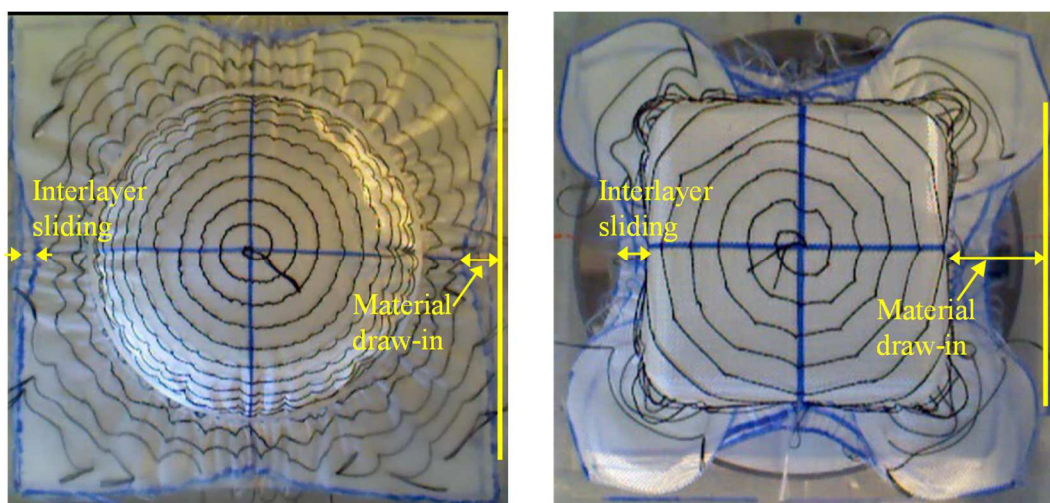
Table 2 Main properties of the test specimens.

Tufting pattern	Ref. of samples	Tufting space (mm)	Tufting angle (°)	Total of tufting points	Areal density (g/m ²)
 Square spiral	S5	5	-	3025	802.3±9.0
	S10	10	-	729	684.9±7.0
	S20	20	-	169	649.2±7.0

 Circle spiral	C10/10	10	10	535	672.2±7.0
	C10/20	10	20	256	659.9±6.0
	C10/30	10	30	182	659.4±5.0
	C20/15	20	15	169	651.8±5.0

3. Forming results

Fig. 7 shows two examples of the deformed tufted preforms after performing. Since all the specimens were stacked in the same sequence, the way of the sample deformation during forming was always quasi-symmetric and similar to each other. To quantify the formability, the maximum material draw-in and the maximum inter-layer sliding were used to be the indicators of the extent of global deformation and different deformation of plies respectively. All the measurement data was obtained as the mean values at the centre of four sides in the Fig.7. In order to improve the understanding of tufted multi-layered preforms and of their formability during manufacturing, in particular, the influence of the tufting pattern, the investigation of forming behaviour of the different tufted preforms will be conducted by analysing the in-plane and out-of-plane characterisations. The measurement data with a good reproducibility was achieved by repeating the same preforming tests (3 tests).



(a)

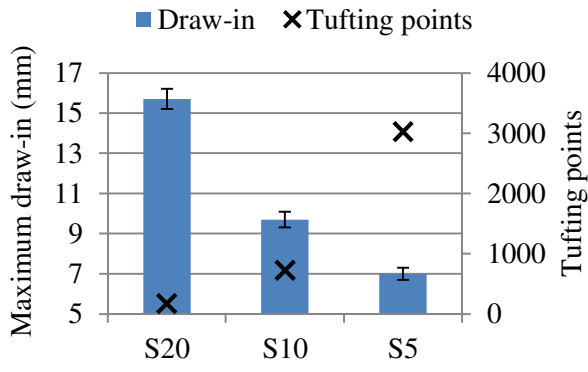
(b)

Fig.7. Deformed tufted preforms after forming, (a) hemispherical forming using C10/10 sample and (b) square-box forming using C10/30 sample.

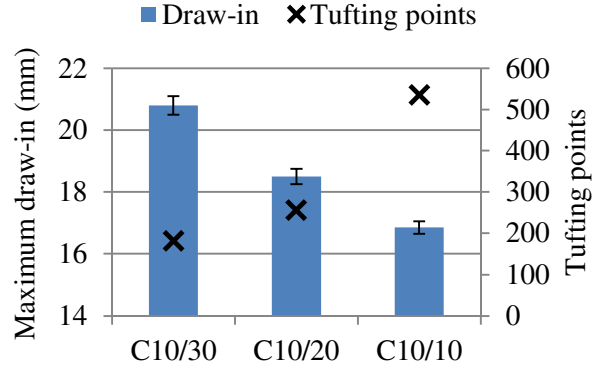
3.1 Material draw-in and punch load

The tufted preforms with different tufting patterns were tested in hemispherical and square-box forming processes. The bar graph and the cross-symbol graph shown in Figs.8a-8d are the representation of the maximum material draw-in and the number of tufting points, respectively. Impact of tufting points can be noted clearly in the figures. The material draw-in decreases with the increasing of the number of tufting points. The inserted thread strengthens the reinforcement through-the-thickness of the preform and the linkage among plies. The tufted preform becomes more rigid and is more difficult to deform when more tufting thread is inserted into the preform, which can be confirmed by the observation of the punch load (captured by a load sensor) in Figs. 9a-9d. For the non-tufted samples (Fig. 8e and Fig. 9e), a larger material draw-in and a lower punch load compared to the tufted samples further reflect this tufting effect. Furthermore, it seems that the C10/30 samples always have similar material draw-in value and punch load value to the non-tufted samples in both forming, as a relatively small number of tufting yarns in the underlying zone of blank-holder cannot prevent effectively the different deformation of each layer.

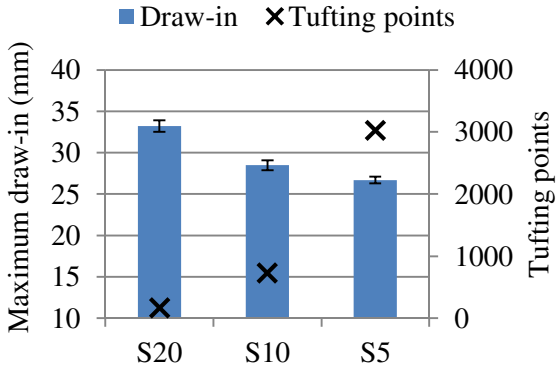
Compared to the S20 sample, the maximum draw-in of S5 sample decreases 56% and 19% for the square spiral pattern after the hemispherical and square-box forming, respectively. In the same way, compared to the C10/30 sample, the maximum draw-in of C10/10 reduces 19% and 9% for circle spiral pattern after the hemispherical and square-box forming, respectively. It can be concluded that the impact of the tufting pattern on the maximum material draw-in in hemispherical forming is always higher than square-box forming.



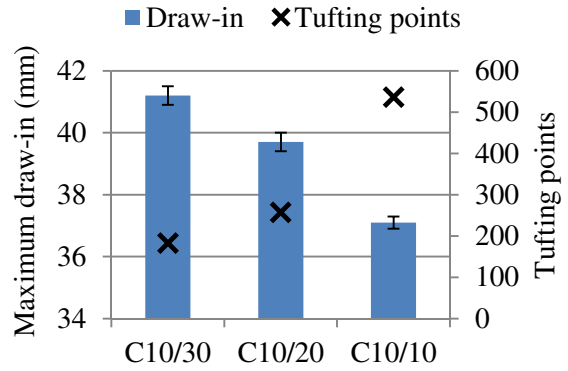
(a) Square spiral pattern/Hemispherical forming



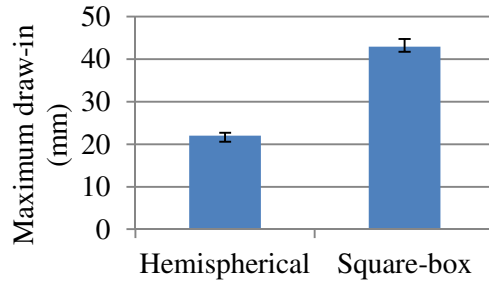
(b) Circle spiral pattern/Hemispherical forming



(c) Square spiral pattern/Square-box forming

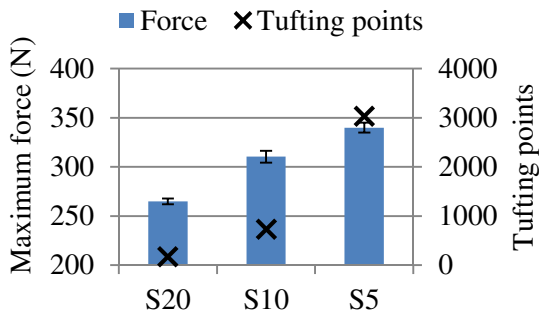


(d) Circle spiral pattern/Square-box forming

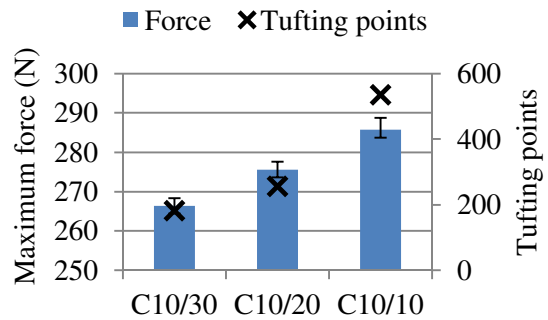


(e) Non-tufted sample in both forming

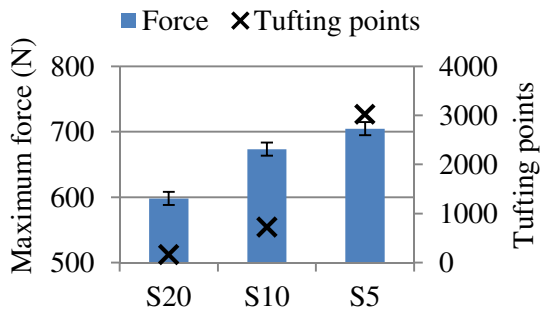
Fig. 8. Influence of tufting pattern and density on the maximum material draw-in in the hemispherical and square-box forming.



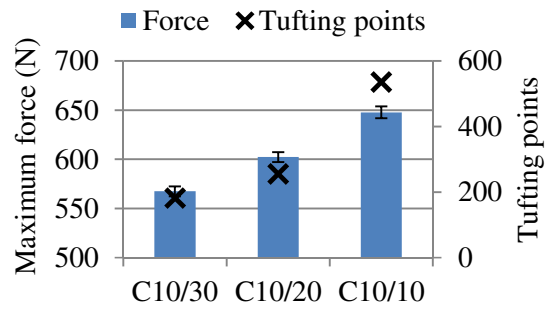
(a) Square spiral pattern/Hemispherical forming



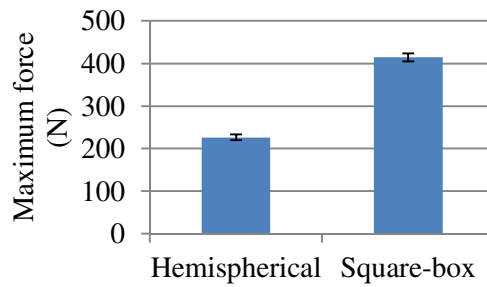
(b) Circle spiral pattern/Hemispherical forming



(c) Square spiral pattern/Square-box forming



(d) Circle spiral pattern/Square-box forming



(e) Non-tufted sample in both forming

Fig. 9. Influence of tufting pattern and density on the maximum punch load in the hemispherical and square-box forming.

3.2 Inter-layer sliding

As one of the important behaviour in the multi-layered forming, inter-layer sliding is mainly caused by the different deformation of each ply and slightly influenced by the changed curvature of each layer, considering the ply thickness. In this test, the maximum measurement value is used to represent the severity of sample inter-layer sliding. Figs.10 shows the inter-layer sliding of preforms during hemispherical and square-box forming. In each group (Fig.10a-d), the inter-layer sliding represented by blue bars is reduced significantly due to the increasing of tufting points. In a certain case, when the tufting points are enough, the tufted preform can be deformed as a single ply (in hemispherical forming with S5 sample).

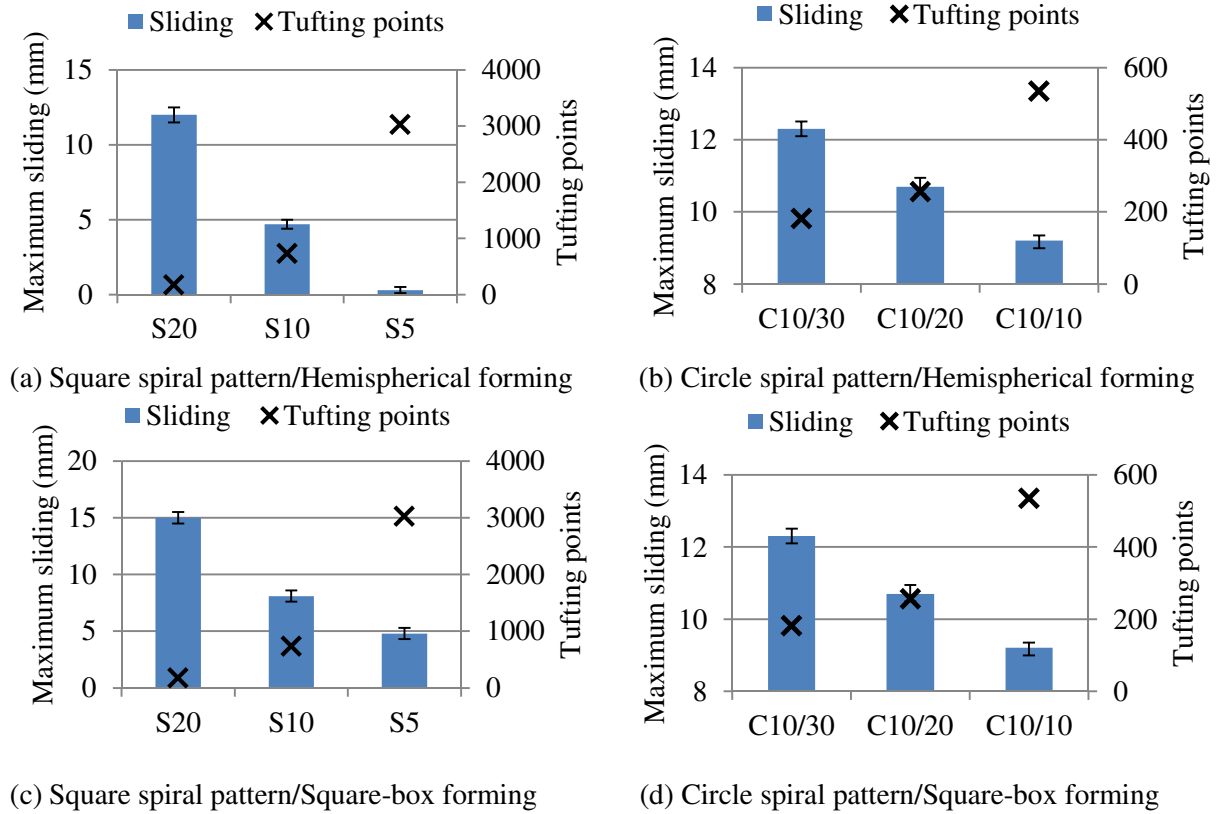


Fig. 10. Influence of tufting pattern and density on the maximum interlayer sliding in the hemispherical and square-box forming.

3.3 Forming defects

3.3.1 Wrinkling

Wrinkling is one of the common defects experienced in the textile composite reinforcements forming. It has a trend to degrade the performance of the final product. Wrinkles occur as the energy needed for an out-of-plane deformation is less than that for an in-plane deformation[4]. The out-of-plane deformation depends on the bending stiffness which is normally weak due to the probable relative motion of fibres. The size of the wrinkles increases along with the bending stiffness[40,41]. However, other parameters can affect wrinkling during forming, such as variations of boundary condition and laminate sequence. Fig.11 shows the forming results of non-tufted samples both in hemispherical and square-box forming. Some large wrinkles with a non-regular shape can be observed in these cases. Previous tests[34] in regard to the square spiral pattern working on the hemispherical punch

reveal that wrinkling phenomenon can be modified by tufting (Figs.12a). Wrinkles are more regularly distributed and the size of wrinkle can be reduced due to the increase of tufting density. This result has been further confirmed by using circle spiral pattern and square-box punch shape.

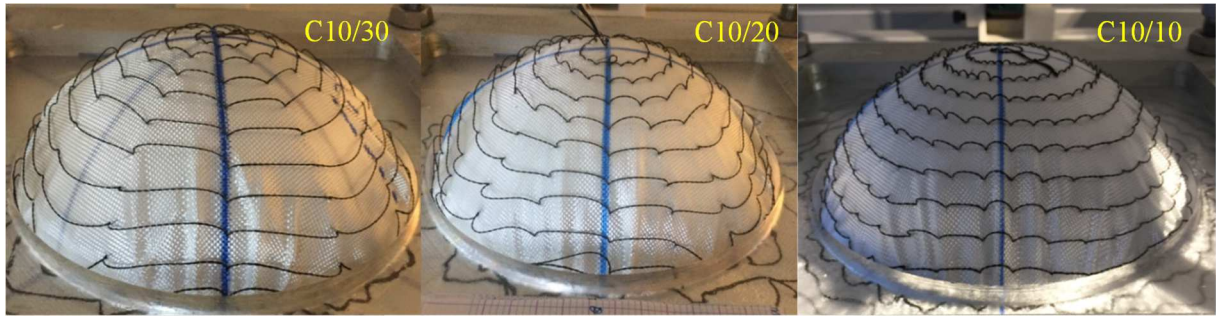


Fig. 11. Wrinkling phenomenon in (a) hemispherical and (b) square-box forming.

Figs.12b show the wrinkling phenomenon magnified in the punch zone and obtained from the preforms tufted in circle spiral pattern during the hemispherical forming. It can be observed that the sizes of wrinkles can be apparently reduced as the decreasing of the tufting angle (increasing of the tufting density). Since the tufting yarn can bond the four plies together, the fabric is hard to bend at the tufting place. The wrinkles normally appear between the tufting points, consequently, the width of wrinkle can be much reduced owing to the decrease of tufting angle.



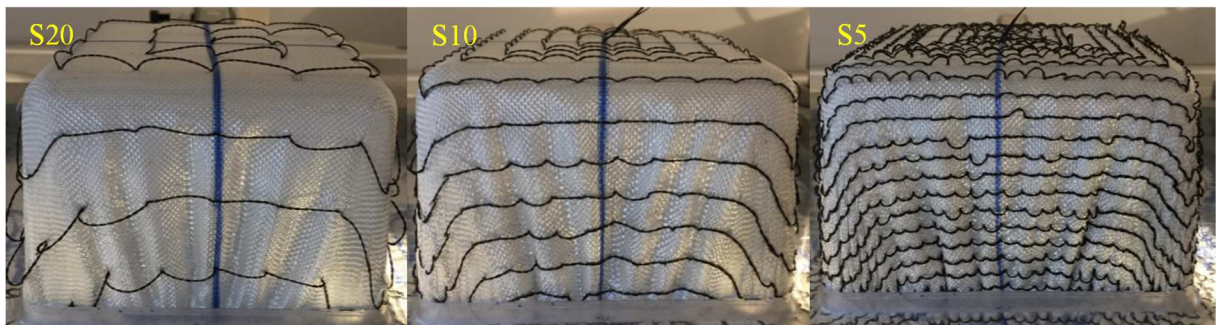
(a) Forming of the tufted preforms with the square spiral pattern



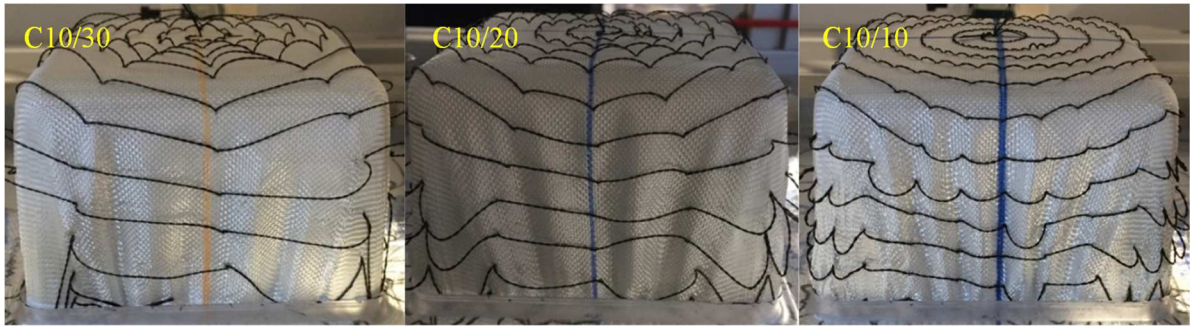
(b) Forming of the tufted preforms with the circle spiral pattern

Fig. 12. Influence of tufting pattern and density on the wrinkling phenomenon in the hemispherical forming.

Compared to the hemispherical forming, the square-box forming can generate a wider range of defects with more significant magnitude. In this deep-draw forming by using the square-box shape, the wrinkles are distributed on the four lateral surfaces. In the case of the square spiral pattern shown in Figs. 13a, it can be concluded that the wrinkles turn to be thinner due to the decrease of tufting space. Figs.13b present the wrinkling phenomena experienced in the square-box forming by using the circle spiral pattern. As observed in Figs. 13a using the square spiral pattern, the reduction of tufting angle of the circle spiral pattern leads to the decrease of the width of the wrinkles.



(a) Forming of the tufted preforms with the square spiral pattern

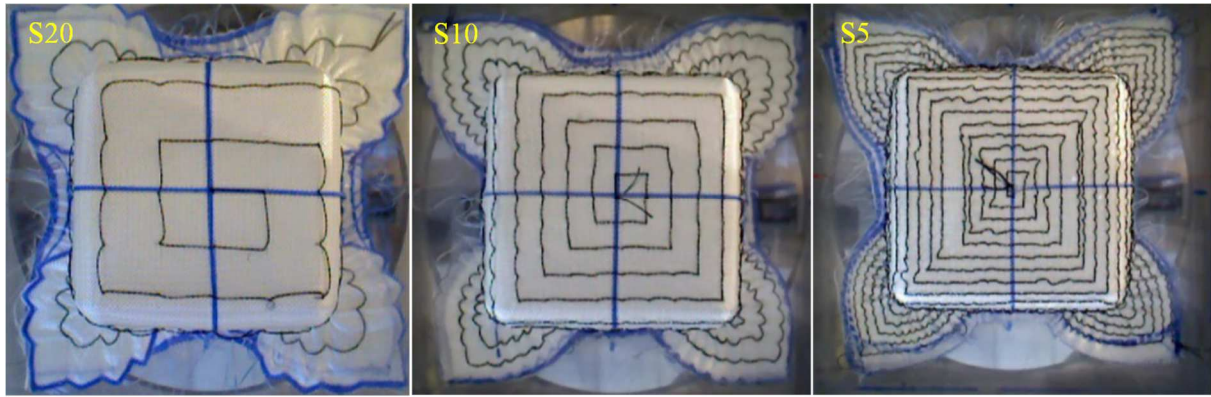


(b) Forming of the tufted preforms with the circle spiral pattern

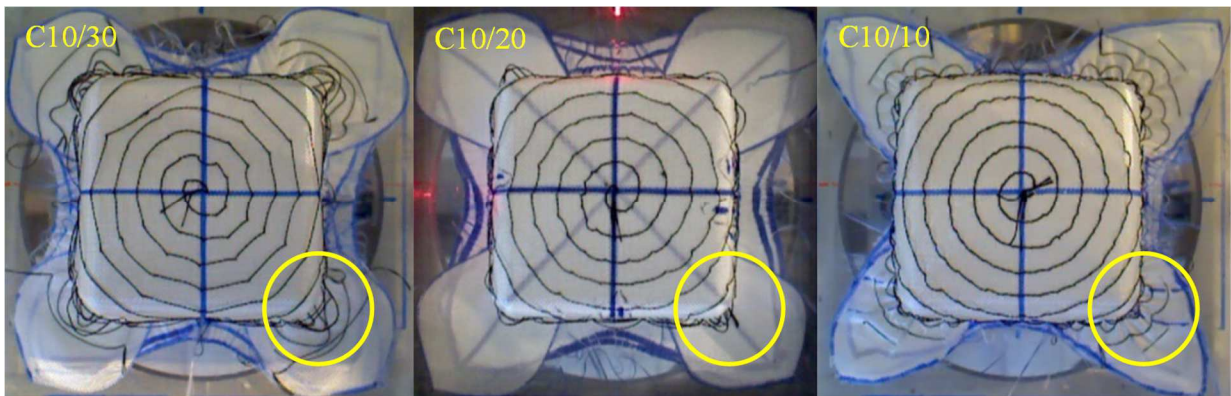
Fig. 13. Influence of tufting pattern and density on the wrinkling phenomenon in the square-box forming.

3.3.2 Out-of-plane defects

Out-of-plane defects identified as the buckles at the scale of tufting yarn can be observed at the four corners in the square-box forming. As noted in Figs. 13b and 14b, these buckles are noted only for the preforms tufted by using the circle spiral pattern. The tufting yarns between two tufting nodes at the corner become curved when the preform accommodates the change of punch geometry. Moreover, the size of buckles can be changed along with the variation of tufting density (see Fig. 14b). Since the fabric is submitted to a high level of shear deformation in the diagonal direction, this high shear deformed state conducts to a decrease of the distance of adjacent tufting points at the four corners. As a result, in these locations, the buckles of tufting yarn appear. In addition, the buckling phenomenon is less important when the tufting angle is small. It can be considered that following the decrease of tufting angle, more tufting points are distributed at the corner of the preform. The initial big buckle can be divided into some small buckles due to the increase of tufting point. On the contrary, when the square spiral pattern is used to accommodate the square-box punch, no distinct buckling phenomenon is observed (Figs. 13a and 14a). As for the square spiral pattern, the tufting yarn is embedded along the weft or warp direction. When the shear deformation takes place at the corner, the distance between two tufting points is not changed too much due to its synchronous deformation caused by the yarn network.



(a) With the square spiral pattern



(b) With the circle spiral pattern

Fig. 14. Top view of the deformed preforms with the different tufting pattern.

4. Discussion about the consistency between tufting pattern and punch shape

In order to analyze the consistency between tufting pattern and punch shape, two types of sample are chosen (S20 and C20/15). Their main parameters are listed in Table.3. The two samples have the same areal density, but the different tufting pattern. Moreover, they have the same total tufting points, but the distribution of tufting points is different for each sample in the punch zone and the underlying zone of blank-holder. Figs. 15 and 16 present the forming results of the S20 and C20/15 tufted reinforcements in both hemispherical and square box manufacturing. It can observe that the forming of the S20 sample is more difficult to achieve compared to that of C20/15 sample. Regarding the main characterizations of S20 and C20/15 samples, it can be considered that the tufting in the zone underlying the blank-holder brings out more limitation between the plies during the forming. It means that the tufted preform is

more rigid and has less movement between the plies when the square spiral pattern is used compared to the circle spiral pattern during both hemispherical and square-box forming. Consequently, with the same areal density, the tufting points in the zone underlying the blank-holder have a more significant impact than the consistency between the tufting pattern and the punch shape.

Regarding the hemispherical case, the small variants can be observed between S20 and C20/15 forming. By contrast, the bigger variants can be remarked in square-box forming. Compared to hemispherical forming, the present square-box forming is a deep-draw forming process in which the preforms are submitted to large deformations. Consequently, the consistency between tufting pattern and punch shape is more important in square-box forming than hemispherical one. The importance of the consistency between the tufting pattern and punch shape should be emphasized in a deep-draw manufacturing process.

Table 3. Main parameters of S20 and C20/15 samples.

Forming	Ref. of samples	Areal density (g/m ²)	Tufting points		
			Total points	Tufting points in punch zone	Tufting points in the zone underlying the blank holder
Hemispherical forming	S20	649.2±7.0	169	97	72
	C20/15	651.8±5.0	169	133	36
Square-box forming	S20	649.2±7.0	169	129	40
	C20/15	651.8±5.0	169	141	28

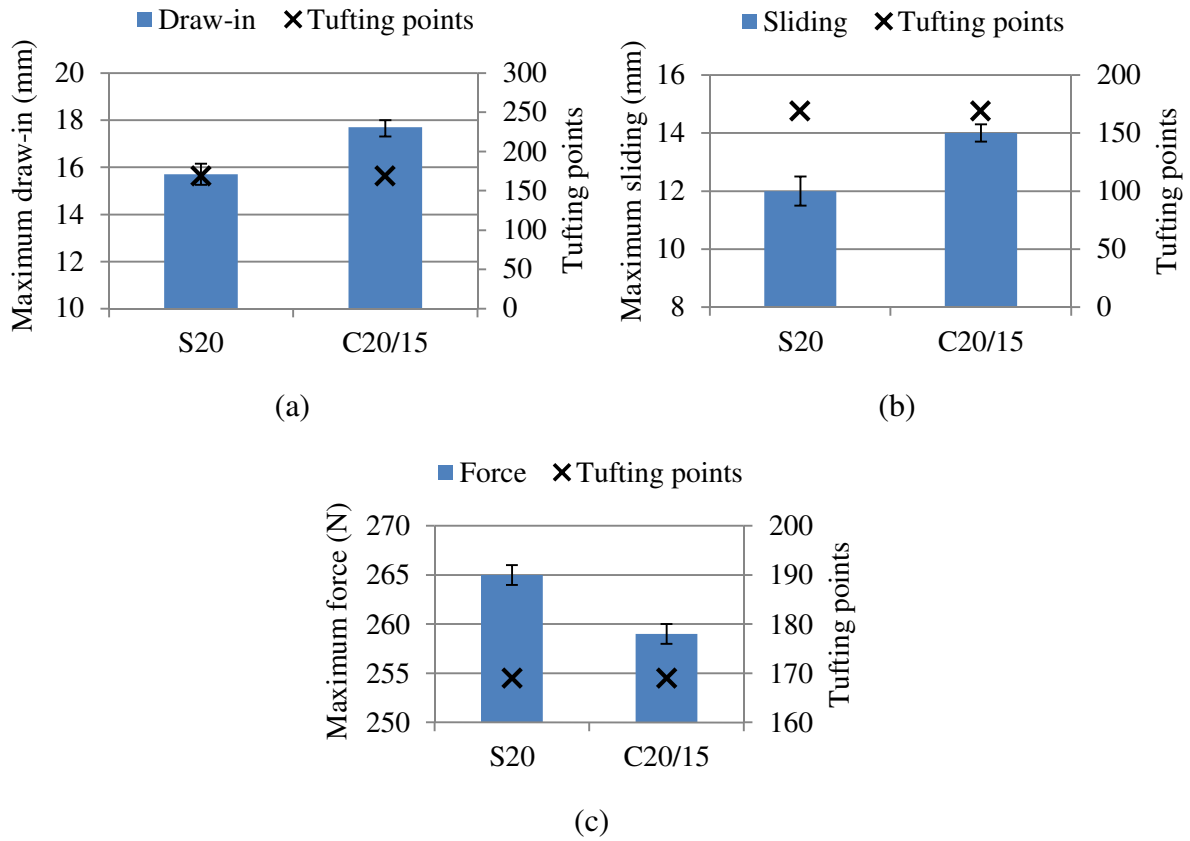


Fig. 15. The comparison of two tufting patterns during hemispherical forming.

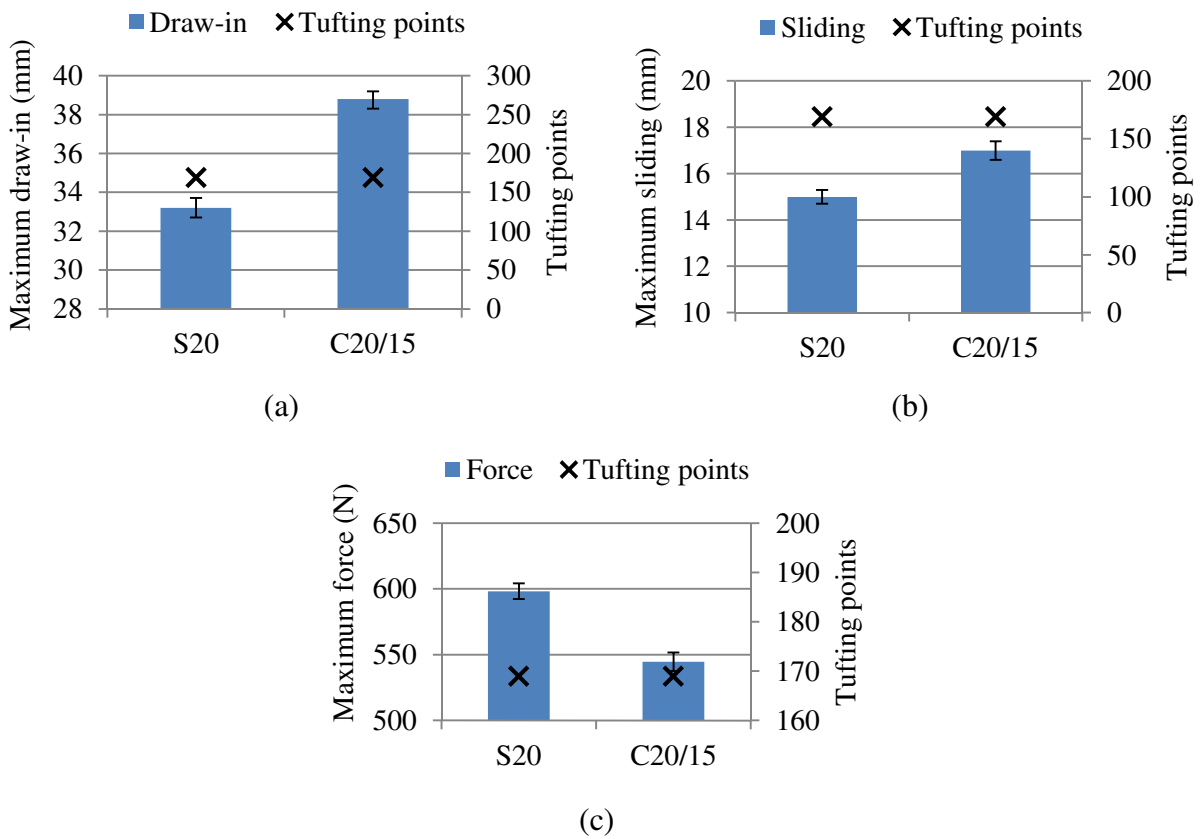
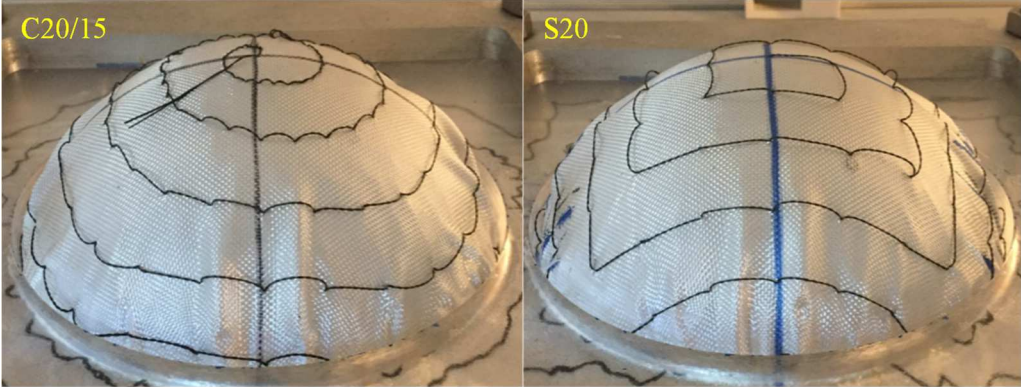
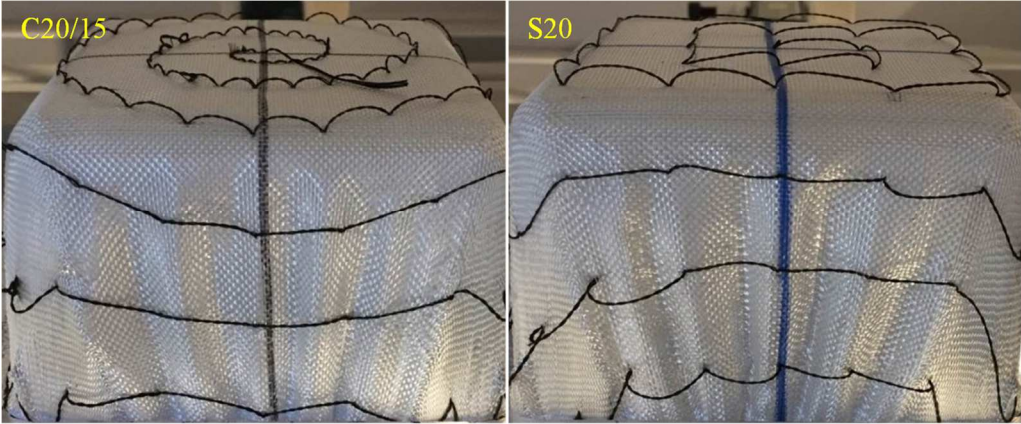


Fig. 16. The comparison of two tufting patterns during square-box forming.

The wrinkling phenomenon can be observed in S20 and C20/15 forming processes. As shown in Fig. 17, it seems that no apparent difference of the number and the position of the wrinkles can be observed during the hemispherical and the square-box forming with the two tufting patterns. By contrast, the width of wrinkles in S20 forming is slightly smaller compared to C20/15 forming. Consequently, the forming results depend more on the number of the tufting points in the zone underlying the blank holder than the tufting pattern.



(a) Hemispherical forming



(b) Square-box forming

Fig. 17. The comparison of wrinkling phenomenon between two tufting patterns.

The out-of-plane defects as the buckles of tufting yarn can be observed in the circle spiral tufted preforms forming, but not in the square spiral tufted preforms forming (see Fig. 18). Therefore, using the square spiral pattern can avoid the generation of out-of-plane defects of tufting yarn localized in the high shear deformation zone. In addition, if the preform is not

submitted to high shear deformation, both two patterns can be applied for tufting. The out-of-plane phenomenon can be mitigated by the reduction of tufting angle in the use of the circle spiral pattern.

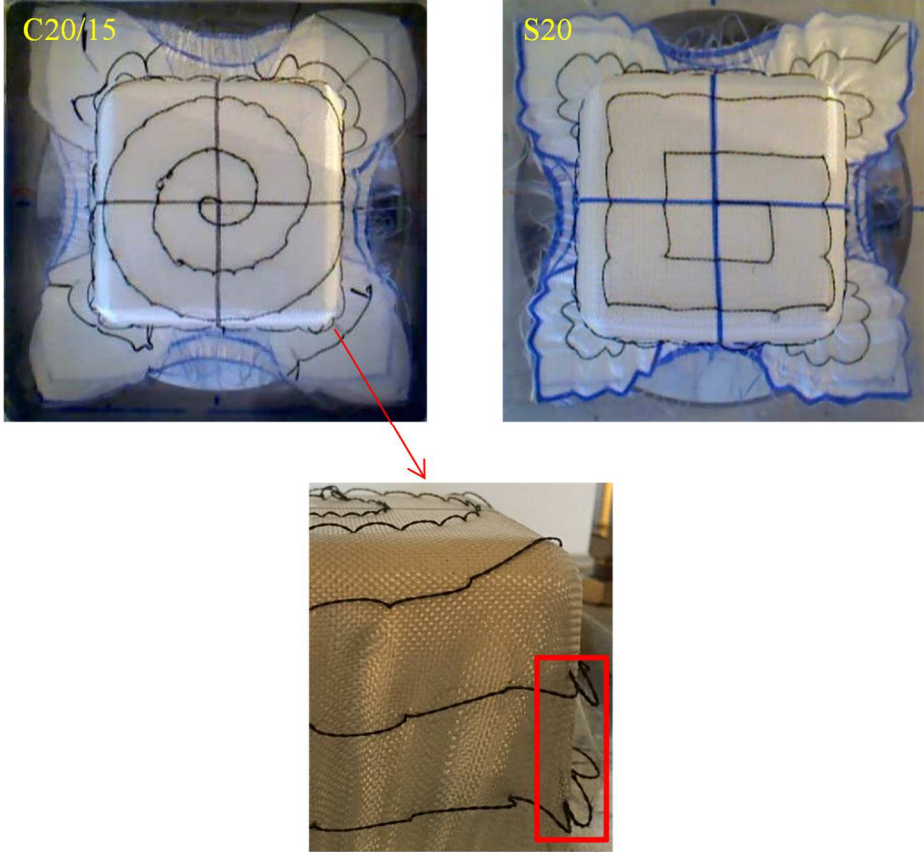


Fig. 18. The out-of-plane defects during in the tufted preforms forming.

5. Conclusion

The present experimental study is focused on the formability behaviours of tufted 3D preforms. The tufted preforms were reinforced by the through-the-thickness tufting yarns. The formability analyses were performed in the hemispherical and square box forming processes. In both two forming processes, when the tufting space decreases, a more rigid preform with less motion between plies can be obtained. Consequently, the material draw-in and the interlayer sliding decrease following the decreasing of the tufting space (the increasing of the number of the tufting points). On another hand, the presence of tufting yarns modified the

wrinkling phenomena of the deformed preform. The decreasing of the tufting space can weaken the wrinkling defects.

The discussion about the consistency between tufting pattern and punch shape shows that there is no significant importance to use the similar tufting pattern to the punch shape. But the circle spiral pattern is not suitable to the square box forming as the out-of-plane defects of the tufting yarns are induced at the corners even if a small tufting space is employed. Moreover, the forming behaviour depends on the number of the tufting points, in particular in the zone underlying the blank holder. From a point of view of the through-the-thickness reinforcements, tufting technology can strengthen the mechanical performance of interlayers in laminated composites. The punch zone of the piece should be completely tufted and the zone underlying the blank holder should be tufted in the effective regions. Consequently, the optimization of the tufted regions in zone underlying the blank holder to minimize the forming defects will be one of the important future works.

References

- [1] Doitrand A, Fagiano C, Leroy FH, Mavel A, Hirsekorn M. On the influence of fabric layer shifts on the strain distributions in a multi-layer woven composite. *Compos Struct* 2016;145:15–25. doi:10.1016/j.compstruct.2016.02.054.
- [2] Rudd CD, Long AC. *Liquid Molding Technologies*, Cambridge: Woodhead Pub 1997.
- [3] Šimáček P, Advani SG. Desirable features in mold filling simulations for liquid composite molding processes. *Polym Compos* 2004;25:355–67. doi:10.1002/pc.20029.
- [4] Allaoui S, Cellard C, Hivet G. Effect of inter-ply sliding on the quality of multilayer interlock dry fabric preforms. *Compos Part A Appl Sci Manuf* 2015;68:336–45. doi:10.1016/j.compositesa.2014.10.017.
- [5] Dufour C, Wang P, Boussu F, Soulat D. Experimental Investigation About Stamping Behaviour of 3D Warp Interlock Composite Preforms. *Appl Compos Mater* 2014;21:725–38. doi:10.1007/s10443-013-9369-9.
- [6] Allaoui S, Hivet G, Soulat D, Wendling A, Ouagne P, Chatel S. Experimental preforming of highly double curved shapes with a case corner using an interlock reinforcement. *Int J Mater Form* 2014;7:155–65. doi:10.1007/s12289-012-1116-5.
- [7] Vanclooster K, Lomov S V, Verpoest I. On the formability of multi-layered fabric composites. *Proc 17th Int Conf Compos Mater* 2009:1–10.
- [8] Harrison P, Gomes R, Correia N, Abdiwi F, Yu WR. Press Forming the Double-Dome Benchmark Geometry Using a 0 / 90 Uniaxial Cross-Ply Advanced Thermoplastic Composite 2012;54:24–8.
- [9] Zhu B, Yu TX, Zhang H, Tao XM. Experimental investigation of formability of

- commingled woven composite preform in stamping operation. *Compos Part B Eng* 2011;42:289–95.
- [10] Pazmino J, Carvelli V, Lomov S V. Formability of a non-crimp 3D orthogonal weave E-glass composite reinforcement. *Compos Part A Appl Sci Manuf* 2014;61:76–83.
- [11] Gereke T, Döbrich O, Hübner M, Cherif C. Experimental and computational composite textile reinforcement forming: A review. *Compos Part A Appl Sci Manuf* 2013;46:1–10. doi:10.1016/j.compositesa.2012.10.004.
- [12] Nosrat-Nezami F, Gereke T, Eberdt C, Cherif C. Characterisation of the shear–tension coupling of carbon-fibre fabric under controlled membrane tensions for precise simulative predictions of industrial preforming processes. *Compos Part A Appl Sci Manuf* 2014;67:131–9.
- [13] Khan MA, Mabrouki T, Vidal-Sallé E, Boisse P. Numerical and experimental analyses of woven composite reinforcement forming using a hypoelastic behaviour. Application to the double dome benchmark. *J Mater Process Technol* 2010;210:378–88. doi:10.1016/j.jmatprotec.2009.09.027.
- [14] Rashidi A, Milani AS. Passive control of wrinkles in woven fabric preforms using a geometrical modification of blank holders. *Compos Part A Appl Sci Manuf* 2018;105:300–9. doi:10.1016/j.compositesa.2017.11.023.
- [15] Liang B, Hamila N, Peillon M, Boisse P. Analysis of thermoplastic prepreg bending stiffness during manufacturing and of its influence on wrinkling simulations. *Compos Part A Appl Sci Manuf* 2014;67:111–22.
- [16] Rashidi A, Milani AS. A multi-step biaxial bias extension test for wrinkling/de-wrinkling characterization of woven fabrics: Towards optimum forming design guidelines. *Mater Des* 2018;146:273–85. doi:10.1016/j.matdes.2018.02.075.
- [17] Ouagne P, Soulat D, Moothoo J, Capelle E, Gueret S. Complex shape forming of a flax woven fabric; analysis of the tow buckling and misalignment defect. *Compos Part A Appl Sci Manuf* 2013;51:1–10.
- [18] Wang P, Hamila N, Boisse P. Thermoforming simulation of multilayer composites with continuous fibres and thermoplastic matrix. *Compos Part B Eng* 2013;52:127–36. doi:10.1016/j.compositesb.2013.03.045.
- [19] Iwata A, Inoue T, Naouar N, Boisse P, Lomov S V. Meso-macro simulation of the woven fabric local deformation in draping. *AIP Conf Proc* 2018;1960. doi:10.1063/1.5034813.
- [20] Wang P, Legrand X, Boisse P, Hamila N, Soulat D. Experimental and numerical analyses of manufacturing process of a composite square box part: Comparison between textile reinforcement forming and surface 3D weaving. *Compos Part B Eng* 2015;78:26–34. doi:10.1016/j.compositesb.2015.03.072.
- [21] Ten Thijs RHW, Akkerman R. A multi-layer triangular membrane finite element for the forming simulation of laminated composites. *Compos Part A Appl Sci Manuf* 2009;40:739–53.
- [22] ten Thijs RHW, Akkerman R. Finite element simulations of laminated composites forming processes. *Int J Mater Form* 2010;3:715–8.
- [23] Fetfatsidis KA, Jauffrès D, Sherwood JA, Chen J, Ten Thijs RHW, Akkerman R, et al. Characterization of the tool/fabric and fabric/fabric friction for woven-fabric composites during the thermostamping process. *Compos Part A Appl Sci Manuf* 2013;6:209–21. doi:10.1016/j.compositesa.2011.03.023.
- [24] Ten Thijs RHW, Akkerman R, Ubbink M, Van Der Meer L. A lubrication approach to friction in thermoplastic composites forming processes. *Compos Part A Appl Sci Manuf* 2011;42:950–60. doi:10.1016/j.compositesa.2011.03.023.
- [25] Alshahrani H, Hojjati M. Bending behavior of multilayered textile composite prepregs:

- Experiment and finite element modeling. *Mater Des* 2017;124:211–24.
doi:10.1016/j.matdes.2017.03.077.
- [26] Nosrat F, Gereke T, Cherif C. Composites : Part A Analyses of interaction mechanisms during forming of multilayer carbon woven fabrics for composite applications. *Compos PART A* 2016;84:406–16. doi:10.1016/j.compositesa.2016.02.023.
- [27] Gnaba I, Legrand X, Wang P, Soulat D. Literature review of tufted reinforcement for composite structures. *IOP Conf Ser Mater Sci Eng* 2017;254. doi:10.1088/1757-899X/254/4/042011.
- [28] Mouritz AP. Review of z-pinned composite laminates. *Compos Part A Appl Sci Manuf* 2007;38:2383–97.
- [29] Mouritz AP, Bannister MK, Falzon PJ, Leong KH. Review of applications for advanced three-dimensional fibre textile composites. *Compos Part A Appl Sci Manuf* 1999;30:1445–61.
- [30] Mouritz AP, Cox BN. A mechanistic interpretation of the comparative in-plane mechanical properties of 3D woven, stitched and pinned composites. *Compos Part A Appl Sci Manuf* 2010;41:709–28.
- [31] M'embre B, Gannon S, Yasae M, Hallett SR, Partridge IK. Mode II delamination resistance of composites reinforced with inclined Z-pins. *Mater Des* 2016;94:565–72. doi:10.1016/j.matdes.2016.01.051.
- [32] Zhang Y, Sun F, Wang Y, Chen L, Pan N. Study on intra/inter-ply shear deformation of three dimensional woven preforms for composite materials. *Mater Des* 2013;49:151–9.
- [33] Gereke T, Cherif C. A review of numerical models for 3D woven composite reinforcements. *Compos Struct* 2018.
- [34] Liu LS, Zhang T, Wang P, Legrand X, Soulat D. Influence of the tufting yarns on formability of tufted 3-Dimensional composite reinforcement. *Compos Part A Appl Sci Manuf* 2015;78:403–11. doi:10.1016/j.compositesa.2015.07.014.
- [35] Cartié DDR, Dell'Anno G, Poulin E, Partridge IK. 3D reinforcement of stiffener-to-skin T-joints by Z-pinning and tufting. *Eng Fract Mech* 2006;73:2532–40. doi:10.1016/j.engfracmech.2006.06.012.
- [36] Dell'Anno G, Treiber JWG, Partridge IK. Manufacturing of composite parts reinforced through-thickness by tufting. *Robot Comput Integr Manuf* 2016;37:262–72. doi:10.1016/j.rcim.2015.04.004.
- [37] Chehura E, Dell'Anno G, Huet T, Staines S, James SW, Partridge IK, et al. On-line monitoring of multi-component strain development in a tufting needle using optical fibre Bragg grating sensors. *Smart Mater Struct* 2014;23. doi:10.1088/0964-1726/23/7/075001.
- [38] Henao A, Carrera M, Miravete A, Castejón L. Mechanical performance of through-thickness tufted sandwich structures. *Compos Struct* 2010;92:2052–9. doi:10.1016/j.compstruct.2009.11.005.
- [39] Labanieh AR, Garnier C, Ouagne P, Dalverny O, Soulat D. Intra-ply yarn sliding defect in hemisphere preforming of a woven preform. *Compos Part A Appl Sci Manuf* 2018;107:432–46. doi:10.1016/j.compositesa.2018.01.018.
- [40] Liang B, Hamila N, Peillon M, Boisse P. Analysis of thermoplastic prepreg bending stiffness during manufacturing and of its influence on wrinkling simulations. *Compos Part A Appl Sci Manuf* 2014;67:111–22. doi:10.1016/j.compositesa.2014.08.020.
- [41] Boisse P, Hamila N, Vidal-Sallé E, Dumont F. Simulation of wrinkling during textile composite reinforcement forming. Influence of tensile, in-plane shear and bending stiffnesses. *Compos Sci Technol* 2011;71:683–92. doi:10.1016/j.compscitech.2011.01.011.